Vol. 5 No. 1 (2026)

Pakistan Journal of Medical & Cardiological Review

https://pakjmcr.com/index.php/1/about

Online ISSN 3007-2387

Print ISSN 3007-2379

Smart Nano-Hydrogels for Self-Healing Dental Restorations: Synthesis, Characterisation, and In Vitro Performance Evaluation

Dr. Hira Rasheed
General Dentist, Dental College HITEC IMS, Taxila

Author Details

Keywords: Nano-Hydrogel, Self-Healing, Dental Restoration, HEMA, TEGDMA, Silver Nanoparticles, Drug Release, Antibacterial, Cytotoxicity, Bond Strength

Received on 10 Dec 2025
Accepted on 08 Jan 2026
Published on 19 Jan 2026

Corresponding E-mail & Author*:
Dr. Hira Rasheed
Email: hirarasheed230@gmail.com

Abstract

Dental restorations often fail prematurely due to secondary caries, marginal microleakage, and mechanical fatigue. Smart nano-hydrogels offer a promising solution by integrating self-healing polymer networks with controlled drug release and enhanced mechanical properties. This study aimed to design and synthesize four novel poly (2-hydroxyethyl methacrylate) (pHEMA) and poly (tetraethylene glycol dimethacrylate) (pTEGDMA)-based nano-hydrogels, evaluating their physicochemical characteristics, pH-responsive swelling, drug release kinetics, self-healing efficiency, antibacterial activity against key cariogenic pathogens, and in vitro cytotoxicity per ISO 10993-5. Marginal integrity and bond strength of restorations were tested under simulated thermocycling. Five experimental groups NH-Ctrl, NH-HEMA, NH-TEGDMA, NH-Ag, and NH-Dual were characterized via dynamic light scattering, FTIR, SEM, and TGA. Swelling was assessed at pH 4.0–7.4, and drug release was modeled using Korsmeyer–Peppas, Higuchi, and zero-order kinetics. NH-Dual demonstrated optimal performance: particle size 155 ± 5 nm, zeta potential −27.9 mV, swelling ratio 183.5% at pH 7.4, Korsmeyer–Peppas exponent 0.55, self-healing efficiency 96.3%, and antibacterial zone of inhibition 21.4 ± 1.1 mm. Cell viability remained above 87.6%, and bond strength after 5,000 thermocycles was 22.1 ± 1.8 MPa. These findings highlight the potential of dual-network, silver-loaded nano-hydrogels for advanced self-healing dental restorations.

Introduction

Background and Clinical Problem

One of the most common chronic diseases is dental caries, which are estimated to be found in 2.3 billion people globally, especially in those with untreated caries of permanent teeth (GBD 2019 Diseases and Injuries Collaborators). Since the introduction of adhesive dentistry and composite resin technologies 30 years ago, the secondary caries at the tooth-restoration margins continues to be the primary reason for the failure of dental restorations. This accounts for 56%–80% of all restorative replacements of posterior teeth (Nedeljkovic et al., 2015). The longevity of a composite resin restoration in clinical practice is typically 5 to 10 years, which is lower relative to amalgam restorations. This is largely due to factors such as polymerization shrinkage stress and marginal microleakage. Moreover, conventional resins cannot respond to mechanical or biological insults after they have been placed (Demarco et al., 2012).

Materials science is really starting to explore a phenomenon which was first described

by Brochu in 2011, where a material can self-repair damage without any external stimuli. Hydrogel, a 3D network of hydrophilic polymer that can absorb water, is a unique class of soft biomaterials that can respond to stimuli on their own. At the nanoscale these smart nano-hydrogels can respond to a pH drop that is characteristic of caries lesion formation. This can be achieved by the controlled release of antibacterial agents, as well as the controlled release of agents that aid in the remineralization, of these lesions (Wu & Mantha, 2017).

The Significance of Nano-Hydrogel-Based Systems

Thanks to rapidly advancing polymer chemistry, it is now possible to synthesize nanotechnology-based hydrogels that can rapidly control swelling and also be used to deliver drugs for a prolonged period of time (Wu, 2017). pHEMA is a polymer that has been widely studied in certain applications for dental and other polymer science fields as a biocompatible polymer that has excellent clarity and has the potential to be compatible with commercially available dental resins (Davis & Anseth, 2002). The poly(ethylene oxide) structure of TEGDMA is a crosslinker that can control the degree of elasticity and swelling of a polymer network. The use of silver nanoparticles in a hydrogel polymer matrix can provide an antimicrobial effect through a number of mechanisms that include the generation of reactive oxygen species as well as the ability to disrupt bacterial cell membranes (Rai et al., 2009). Aside from a number of studies that have examined several of the listed properties separately, no other research has extensively studied a dual network nano-hydrogel system that integrates pH responsive HEMA/TEGDMA with AgNPs for dental restoration applications. Simultaneously, it has yet to analyze the numerous properties listed including healing of physical defects, in vitro release of drugs and the evaluation of antibacterial activity as well as cytotoxicity according to ISO standards, and the mechanical properties of the hydrogels under the influence of thermocycling.

Research Objectives

The primary objectives of this investigation were to: (1) synthesise and physicochemically characterise five nano-hydrogel formulations; (2) determine pH-responsive swelling kinetics over a clinically relevant pH range of 4.0–7.4; (3) model in vitro drug release profiles using established mathematical kinetic models; (4) quantify self-healing efficiency over multiple healing cycles; (5) assess antibacterial activity against S. mutans, L. acidophilus, S. aureus, E. faecalis, and C. albicans; (6) evaluate biocompatibility per ISO 10993-5 on L929 fibroblast cells; and (7) measure marginal microleakage and bond strength after accelerated thermocycling.

Hypotheses

H_1: NH-Dual will exhibit significantly higher swelling ratios at acidic pH compared to single-monomer formulations.

H_2: AgNP-containing formulations will produce statistically larger zones of inhibition against all tested cariogenic organisms.

H_3: Self-healing efficiency will remain above 85% for at least five consecutive healing cycles.

H_4: All formulations will demonstrate cell viability >70% at concentrations ≤ 250 µg/mL, classifying them as non-cytotoxic per ISO 10993-5 Grade 1.

Literature Review

Evolution of Dental Restorative Materials

The history of dental restorative materials spans over a century, evolving from amalgam and gold restorations toward tooth-coloured resin composites in the late 1960s following the introduction of the bis-GMA monomer system by Bowen (1963).

Contemporary resin composites consist of a dimethacrylate monomer matrix, inorganic filler particles, a coupling agent (typically γ-methacryloxypropyltrimethoxysilane), photoinitiators, and stabilisers. The progressive miniaturisation of filler particles from macro-fillers (>10 μm) through hybrid and microhybrid systems to nanofilled composites (particle diameter <100 nm) has improved polishability and surface smoothness without commensurate improvements in marginal adaptation or secondary caries prevention (Ferracane, 2011).
All current composite systems have an inert and static limitation after being polymerised. Biological hard tissues, in contrast, have some degree of self-healing mechanisms and can be remineralised, whereas conventional dental restorations lack the ability to self-modulate and counter the effects of the acidic microenvironment of the cariogenic biofilm induced at the margin of the restoration. These limitations of the conventional restorations have led to research and development of active restorative materials which can respond and adjust to the varying conditions.

Hydrogel Science: Fundamentals and Classifications
Hydrogels are materials that consist of a three-dimensional network of crosslinked hydrophilic polymers which can swell. Among various descriptions, hydrogels can be classified based on their source of polymers (natural or synthetic), or based on the mechanism of polymer crosslinking (physically or chemically crosslinked). Furthermore, they can be classified based on their responsiveness to external stimuli (temperature, pH, light, glucose) and based on the arrangement of their polymer chains, for instance, copolymeric, semi-interpenetrating, and full interpenetrating networks. Hydrogels which are responsive to pH changes, the most relevant type of hydrogels in dentistry for the management of dental caries, contain ionisable pendants (commonly weak carboxylic acids or weak bases, like amines). These pendant chains can either be protonated or deprotonated, which results in a dramatic volume change of the hydrogel network (Hoffman, 2012).
For hydrogels that exhibit swelling, the Flory–Rehner theory of swelling equilibrium, along with the Donnan equilibrium, can help explain the thermodynamics and conditions around hydrogel swelling. For polyelectrolyte hydrogels, swelling occurs through an elastic strain of the polymer network which is countered by the mixing thermodynamics of the polymer and solvent. This is also countered by electrostatic repulsion of the fixed polymer chains. The design of polyelectrolytes for hydrogels can be achieved by balancing mixing thermodynamics of polymer and solvent, deign and crosslinking of the polymer chains. These approaches have a great deal of promise for designing hydrogels that can volumetrically change in a predictable and consistent manner (Peppas et al., 2000).

HEMA- and TEGDMA-Based Systems in Dentistry
Poly(2-hydroxyethyl methacrylate) has been examined in dentistry since the 1960s, mainly as a hydrophilic element of dentinal adhesive primers and bonding agents. Polymers with structure similar to pHEMA possess side chain hydroxy groups that encourage wettability and allow hydrogen bonding to collagen fibrils in the dentinal hinterland. Additionally, pHEMA has an adequate glass-transition temperature and excellent optical properties. Due to its Water uptake, pHEMA plasticizes resulting in a matrix that possesses poor mechanical properties. Copolymerization with hydrophobic or crosslinking monomers can potentially address this issue (Sideridou & Achilias, 2005).
TEGDMA is considered a crosslinking diluent as it reduces the viscosity of the monomer system in resin composites, and at the same time, increases the crosslinking density of the resin. At elevated levels, TEGDMA promotes water absorption and hydrolytic deterioration. There are several studies that conclude that HEMA-based

copolymers that contain 10–15 wt% of TEGDMA offer a favorable compromise of polymer network stiffness, swelling, and hydrolytic stability (Gauthier et al., 2005). Therefore, the combination of HEMA and TEGDMA in a nano-hydrogel system is believed to offer the correct balance of mechanical strength and pH-responsive swelling for dental restoration purposes.

Silver Nanoparticles as Antibacterial Agents in Dental Materials

The antimicrobial properties of silver were first studied in ancient times. Nanotechnology plays an important role in synthesizing silver nanoparticles (AgNPs) of controlled sizes (1-100 nm) and surface modifications. In result, biological activity of their mass and concentration are increased. There are several mechanisms in which silver nanoparticles exhibit antimicrobial properties: (1) release of silver ions, which react and bind to thiol groups on bacterial proteins, (2) direct interactions and disruptions of the membrane of bacterial cells, (3) generation of reactive oxygen species (ROS) within the bacteria, and (4) disruption of ATP synthesis and inhibition of bacterial DNA replication (Rai et al., 2009; Leid et al., 2012).

In response to the demand of antibacterial products, silver nanoparticles have been incorporated within various systems of restorative dental materials including, glass ionomer cements, composite resins, and adhesive systems. In the dental field, the main concern is the tradeoff between achieving antibacterial concentrations (minimum inhibitory concentrations (MICs) of 1-10 μg/mL against S. mutans) while preserving the biocompatibility of the silver nanoparticles (AgNPs). Zhang et al. (2021) showed that AgNPs incorporated in methacrylic hydrogels at <= 5 μg/mL maintained L929 fibroblast cell viability > 80% and showed zone of inhibition against S. mutans of 18-22 mm. The hydrogels in the system may provide controlled and sustained release of AgNPs, that incorporate sustained antibacterial activity for a longer duration of time (> 1-2 days) and may overcome the burst release of nanoparticles.

Self-Healing Polymers: Mechanisms and Dental Applications

Self healing materials can be split into two categories: microencapsulated healing materials, which release a healing agent to heal the material when a fracture occurs, and internally sustained materials, which can heal themselves through reversible chemical changes that occur naturally. For the use of dental materials, self healing mechanisms that are based on reversible noncovalent interactions such as hydrogen bonding, π–π stacking, hydrophobic interactions, and metal–ligand coordination, are especially interesting, as they can be used for self healing for an indefinite number of times without the depletion of a self healing agent (White et al., 2001; Brochu et al., 2011).

Self healing polymeric dental materials have been studied through disulfide bond exchange, Diels–Alder cycloaddition, boronic ester exchange, and ureidopyrimidinone (UPy) hydrogen bonding. Hydrogels have a high water content, allowing chain mobility which facilitates the diffusion of a polymer chain and the reformation of the bond that was broken. Autonomously healing hydrogels were first studied swelling at 37°C to reorganize hydrophobic domains (Temenoff and Mikos, 2000). Wu et al. (2022) reported healing efficiencies of over 90% for HEMA-co-acrylic acid hydrogels through targeted hydrogen bonding and electrostatic interactions, indicating that HEMAbased nano-hydrogels may provide self healing capabilities in a clinical setting.

In Vitro Testing Standards and Drug Release Modelling

Biocompatibility assessment of dental materials follows ISO 10993-5 (Tests for In Vitro Cytotoxicity), which specifies that materials with cell viability >70% relative to

negative controls are classified as non-cytotoxic (Grade 0–1). The MTT [3-(4,5-dimethylthiazol-2-yl)-2,5-diphenyltetrazolium bromide] assay on L929 mouse fibroblasts is the gold-standard cytotoxicity test for dental biomaterials. Drug release from polymer matrices is commonly modelled using zero-order (constant release), first-order (concentration-dependent release), Higuchi (diffusion-controlled release from matrix), and Korsmeyer–Peppas (power-law, mechanism-discriminating) kinetic equations. The Korsmeyer–Peppas exponent $n < 0.45$ indicates Fickian diffusion; $0.45 < n < 0.89$ anomalous transport; and $n > 0.89$ Case II relaxation-controlled transport (Korsmeyer et al., 1983).

Material and Methods

Ethical Approval and Study Design

This study was conducted in full compliance with institutional guidelines for in vitro research. No human or animal subjects were involved. All cytotoxicity assays were performed using the commercially available L929 mouse fibroblast cell line (ATCC CCL-1). The study followed a randomised comparative design with five independent experimental groups and a minimum of $n = 8$ replicates per outcome measure. All experiments were conducted in triplicate and data are presented as mean ± standard deviation.

Materials

2-Hydroxyethyl methacrylate (HEMA, ≥99%), tetraethylene glycol dimethacrylate (TEGDMA, ≥95%), N,N-methylenebisacrylamide (MBA, crosslinker), ammonium persulfate (APS, initiator), silver nitrate ($AgNO_3$, ≥99.9%), sodium borohydride ($NaBH_4$, reducing agent), and all analytical-grade solvents were purchased from Sigma-Aldrich (St. Louis, MO, USA). Phosphate-buffered saline (PBS) tablets, acetate buffer components, DMEM cell culture medium, foetal bovine serum (FBS), penicillin-streptomycin, and MTT reagent were sourced from Thermo Fisher Scientific (Waltham, MA, USA). A commercial nanofilled resin composite (Filtek Z350 XT, 3M ESPE) served as the clinical control for mechanical and microleakage comparisons.

Synthesis of Silver Nanoparticles

AgNPs were synthesised by the chemical reduction method. Briefly, 50 mL of 1 mM $AgNO_3$ aqueous solution was prepared and maintained at 4°C under continuous magnetic stirring at 400 rpm. Ice-cold 10 mM $NaBH_4$ (10 mL) was added dropwise over 30 minutes under nitrogen atmosphere to prevent oxidation. Formation of AgNPs was confirmed by the appearance of a characteristic pale-yellow colour and UV-Vis absorbance peak at 397–403 nm (Cary 60, Agilent Technologies). The resulting colloidal suspension was centrifuged at 12,000 rpm for 20 minutes, washed three times with ultrapure water, lyophilised (Labconco FreeZone 6L), and stored at −20°C under nitrogen until use. Particle size and surface plasmon resonance were characterised by transmission electron microscopy (TEM, JEOL JEM-2100F, 200 kV).

Nano-Hydrogel Synthesis and Formulation

Five formulations were synthesised as follows. NH-Ctrl: 10 wt% HEMA, 2 wt% MBA in PBS (pH 7.0); NH-HEMA: 20 wt% HEMA, 3 wt% MBA; NH-TEGDMA: 10 wt% HEMA, 10 wt% TEGDMA, 3 wt% MBA; NH-Ag: 20 wt% HEMA, 3 wt% MBA, 2 µg/mL AgNPs; NH-Dual: 10 wt% HEMA, 10 wt% TEGDMA, 3 wt% MBA, 5 µg/mL AgNPs. All formulations contained 0.1 wt% APS as thermal initiator. Polymerisation was conducted in capped glass vials under nitrogen at 70°C for 4 hours. After synthesis, hydrogels were transferred to dialysis membranes (MWCO 12–14 kDa) and dialysed against ultrapure water for 72 hours (water changed every

12 h) to remove unreacted monomers, initiator residues, and free AgNPs. Nano-hydrogel dispersions were obtained by probe sonication (Branson SFX 250, 40% amplitude, 30 s on/off cycles, 5 minutes total, 0°C ice bath) and filtered through 0.45 µm syringe filters.

Physicochemical Characterisation

Hydrodynamic diameter and polydispersity index (PDI) were determined by DLS (Zetasizer Nano ZS, Malvern Instruments) at 25°C, 173° backscatter angle. Zeta potential was measured in 1 mM KCl. FTIR spectra were acquired on a Nicolet iS5 spectrometer (4000–400 cm^{-1}, 64 scans, 4 cm^{-1} resolution) using the ATR accessory. TGA was conducted on a TA Instruments Q600 (N_2 atmosphere, 10°C/min, 25–600°C). SEM imaging of lyophilised hydrogels was performed on a Zeiss Sigma 300 FE-SEM (5 kV accelerating voltage; gold sputter-coated, 5 nm). Encapsulation efficiency was calculated as (mass of drug/AgNPs encapsulated ÷ total mass of drug/AgNPs added) × 100%.

pH-Responsive Swelling Studies

Cylindrical hydrogel discs (diameter 8 mm, height 2 mm) were prepared and lyophilised to obtain xerogel samples of known dry mass (Wd). Samples were immersed in buffer solutions of pH 4.0, 5.5, 6.5, 7.0, and 7.4 (acetate buffer for pH < 6.0; phosphate buffer for pH ≥ 6.0, 37°C, n = 6 per group per pH). At pre-determined time intervals (0.5, 1, 2, 4, 8, 12, 24 h), samples were removed, surface-blotted with filter paper, and weighed (Ws). Swelling ratio (SR%) = [(Ws − Wd)/Wd] × 100%. Equilibrium SR was defined as the value at 24 h when <2% change was observed between consecutive measurements.

In Vitro Drug Release Modelling

Fluorescein isothiocyanate (FITC, λex = 490 nm, λem = 520 nm) was used as a model drug for optical quantification. Drug-loaded discs were placed in phosphate buffer saline (pH 6.8, 37°C, 100 rpm orbital shaker, n = 6). At each time point (0, 0.5, 1, 2, 4, 6, 8, 12, 24, 48, 72 h), 1 mL aliquots were withdrawn and replaced with fresh buffer. Fluorescence was measured on a Synergy H1 plate reader (BioTek). Cumulative drug release was plotted as $M_t/M_\infty \times 100\%$. Data were fitted to zero-order, first-order, Higuchi, and Korsmeyer–Peppas models using non-linear regression (GraphPad Prism 9.4). Model selection was based on highest R^2 and lowest Akaike Information Criterion (AIC). For AgNP release, ICP-OES (Agilent 5800) was used to measure silver concentration in release medium.

Self-Healing Efficiency Assessment

Nano-hydrogel films (20 × 5 × 1 mm) were cast between glass slides and allowed to equilibrate at 37°C in PBS. A controlled micro-crack was introduced using a steel razor blade (Feather, Japan) under stereomicroscope guidance (Olympus SZ61). Samples were photographed immediately after incision (t_0) and at 2, 4, 6, and 24 hours under identical optical conditions using an optical profilometer (Bruker ContourGT-X). Crack width was measured at 10 equidistant points along each crack using ImageJ 1.53 (NIH). Healing efficiency (HE%) was calculated as [(initial crack width – residual crack width)/initial crack width] × 100%. Mechanical recovery was quantified by nano-indentation (Hysitron TI 950, 50 µN load) before and after healing, calculating the percentage recovery of reduced modulus.

Antibacterial Testing

Antibacterial activity was assessed by the Kirby–Bauer disk diffusion method on Mueller–Hinton agar (MHA) for bacterial strains and Sabouraud Dextrose Agar (SDA)

for C. albicans. Test organisms: Streptococcus mutans (ATCC 25175), Lactobacillus acidophilus (ATCC 4356), Staphylococcus aureus (ATCC 25923), Enterococcus faecalis (ATCC 29212), and Candida albicans (ATCC 10231) were obtained from the Department of Microbiology, University of Karachi. Inoculum suspensions were standardised to 0.5 McFarland (1.5×10^8 CFU/mL). Nano-hydrogel-impregnated discs (6 mm diameter, 100 µL of each formulation) were placed on inoculated plates and incubated at 37°C for 24–48 hours. Zones of inhibition (ZOI, mm) were measured by digital callipers (n = 8 replicates per formulation per organism). Chlorhexidine gluconate (0.2%, positive control) and sterile PBS (negative control) discs were included in each batch.

Cytotoxicity Assay (ISO 10993-5)

L929 mouse fibroblasts were cultured in DMEM supplemented with 10% FBS and 1% penicillin-streptomycin at 37°C, 5% CO_2. Cells were seeded at 1×10^4 cells/well in 96-well plates and allowed to adhere for 24 h. Elution extracts were prepared by immersing 1 cm^2 of each hydrogel per 1 mL of DMEM at 37°C for 24, 48, and 72 h (ISO 10993-12 method). Serial two-fold dilutions (31.25–500 µg/mL) were applied to cells for 24, 48, and 72 h. Cell viability was determined by MTT assay (20 µL of 5 mg/mL MTT per well, 4 h incubation; formazan dissolved in 150 µL DMSO). Absorbance was measured at 570 nm (reference 650 nm) on a microplate reader (BioTek EL808). Viability% = (OD sample/OD negative control) × 100%. Materials were classified per ISO 10993-5 Grade 0 (>90%), Grade 1 (75–90%), Grade 2 (50–75%), or Grade 3 (<50%).

Microleakage and Bond Strength Testing

Sound, freshly extracted human premolar teeth (n = 40, ethics approval exempted for in vitro use, all teeth deidentified) were stored in 0.5% chloramine-T at 4°C and used within 1 month. Class V cavities (3 × 2 × 1.5 mm) were prepared on the buccal surface using a high-speed handpiece under water spray. Teeth were randomly assigned to five groups (n = 8): Conventional RC (control), NH-HEMA, NH-TEGDMA, NH-Ag, and NH-Dual. Nano-hydrogel dispersions were applied as a pre-treatment layer (30 s, light-cured 20 s), followed by conventional composite placement and curing per manufacturer protocol. Specimens were thermocycled (5°C–55°C, 30-second dwell, 0, 500, 1,000, and 5,000 cycles) per ISO 11405. Microleakage was assessed using 2% methylene blue dye penetration (24 h), followed by sectioning and scoring on a 0–3 scale. Shear bond strength was measured using a universal testing machine (Zwick/Roell Z010, 1 mm/min crosshead speed). Failure modes were assessed by stereomicroscopy (n = 6 per group): adhesive, cohesive, and mixed.

Statistical Analysis

All statistical analyses were performed in IBM SPSS Statistics v27. Data normality was verified by Shapiro–Wilk test ($p > 0.05$ for all primary variables). Homogeneity of variance was confirmed by Levene test. Group differences were compared by one-way ANOVA followed by Tukey HSD post-hoc test ($\alpha = 0.05$). Kruskal–Wallis test with Dunn post-hoc correction was applied to non-parametric microleakage scores. Pearson correlation coefficients were calculated between swelling ratio and drug release variables. Effect sizes were reported as partial eta-squared (η^2). All data are reported as mean ± SD unless otherwise stated; $p < 0.05$ was considered statistically significant.

Results

the complete findings from physicochemical characterisation, swelling kinetics, drug

release modelling, self-healing efficiency, antibacterial testing, cytotoxicity assessment, and mechanical/microleakage testing of all five nano-hydrogel formulations. All primary endpoints demonstrated statistically significant inter-group differences ($p < 0.001$). Seven high-resolution three-dimensional graphical analyses and ten data tables are presented. All instruments used for data collection and analysis are specified alongside the respective results. Statistical analysis was conducted using IBM SPSS v27; kinetic modelling was performed using GraphPad Prism 9.4; particle size analysis used Malvern Zetasizer ZEN3600 software; and image quantification was performed with ImageJ 1.53 (NIH).

Physicochemical Characterisation of Nano-Hydrogel Formulations

Dynamic light scattering (DLS) and zeta potential measurements demonstrated a progressive improvement in colloidal stability from NH-Ctrl to NH-Dual. The NH-Ctrl formulation exhibited the largest hydrodynamic diameter (248 ± 12 nm) and highest PDI (0.38 ± 0.03), indicative of a polydisperse colloidal system with suboptimal stability. In contrast, NH-Dual achieved a hydrodynamic diameter of 155 ± 5 nm and PDI of 0.15 ± 0.01, consistent with a narrow, unimodal size distribution. The Zeta potential values was found to be getting increasingly negative in the formulation series, that is, −8.4 ± 1.2 mV for NH-Ctrl to −27.9 ± 1.6 mV for NH-Dual which has AgNP, indicating increased electrostatic repulsion in the dual-monomer, AgNP loaded system. The values less than −25 mV are usually identified as a good colloidal stability (Bhattacharjee, 2016).

The trend of equilibrium water content was similar: 42.1 ± 2.3% (NH-Ctrl) vs. 76.5 ± 2.7% (NH-Dual). The greater water uptake observed in NH-Dual is the result of both the hydroxyl group of HEMA and the more open TEGDMA crosslinked network, allowing for increased water uptake without loss of structural integrity. It was confirmed that the polymerisation was successful in all formulations using FTIR as the carbonyl (C=O ester) peak at 1720 cm^{-1} was still present while the C=C stretching vibration disappeared. The incorporation of Ag was confirmed by the UV-Vis SPR peak for NH-Ag which was observed at 399 nm and for NH-Dual observed at 403 nm (data not shown). All formulations were spherical with smooth surfaces as seen under SEM imaging and NH-Dual had the most uniform particle distribution with no aggregates visible at ×50,000 magnification.

Table 1. Physicochemical Characteristics of All Five Nano-Hydrogel Formulations

Parameter	NH-Ctrl	NH-HEMA	NH-TEGDMA	NH-Ag	NH-Dual
Particle Size (nm)	248 ± 12	185 ± 9	172 ± 7	162 ± 6	155 ± 5
PDI	0.38 ± 0.03	0.24 ± 0.02	0.19 ± 0.01	0.17 ± 0.01	0.15 ± 0.01
Zeta Potential (mV)	–8.4 ± 1.2	–18.6 ± 1.4	–22.3 ± 1.1	–25.7 ± 1.3	–27.9 ± 1.6
Water Content (%)	42.1 ± 2.3	67.4 ± 2.1	71.2 ± 1.9	73.8 ± 2.4	76.5 ± 2.7
Cross-link Density (%)	8.2 ± 0.4	12.5 ± 0.6	15.8 ± 0.7	14.3 ± 0.5	16.1 ± 0.8
pH at synthesis	7.0	7.0	7.0	7.0	7.0
Encap. Efficiency (%)	N/A	78.3 ± 2.6	82.1 ± 3.1	84.7 ± 2.8	87.2 ± 3.4

Note. Data presented as mean ± SD (n = 6). NH-Ctrl = control hydrogel (baseline HEMA); NH-HEMA = enhanced HEMA formulation; NH-TEGDMA = TEGDMA crosslinked; NH-Ag = silver nanoparticle-loaded; NH-Dual = combined

HEMA/TEGDMA with AgNPs. PDI = polydispersity index. Encapsulation efficiency was not applicable (N/A) for NH-Ctrl. All groups significantly different from NH-Ctrl by one-way ANOVA + Tukey HSD ($p < 0.05$). Characterisation tools: DLS (Malvern Zetasizer Nano ZS); FTIR (Nicolet iS5 ATR); SEM (Zeiss Sigma 300 FE-SEM); TGA (TA Instruments Q600).

pH-Responsive Swelling Kinetics

All the nano hydrogels showed characteristic swelling properties which increased with the pH and were higher at alkaline pH than acidic pH, resulting from the ionisation of the carboxylate groups in the backbone of the polyacrylate. This inverse pH-swelling relationship is clinically desirable as low pH (4.5-5.5) at the restoration margin would occur if the early carious lesion occurs, and this would stimulate moderate contraction of the network and increased release of the drug to deal with the cariogenic challenge. At physiological pH (7.4), by contrast, optimal network expansion enables mechanical adaptation and sealing of the gaps.

NH-Dual had the largest value of equilibrium swelling ratio at all studied pH values with the highest value at 183.5 ± 7.6% at pH 7.4 after 24 hours and 88.1 ± 3.9% at pH 4.0 after 24 hours. The lower the swelling values, the less is the density of the cross-links and there are no pH responsive ionisable groups, as in the case of NH-Ctrl (88.1% for pH 7.4 and 18.2% for pH 4.0). The swelling kinetics were biphasic, comprising fast initial swelling in the first 1–2 h followed by a slower swelling to equilibrium by 12–24 h. This behaviour is well described by the modified Fickian diffusion model for swelling controlled transport (Peppas & Bures, 2004). The pH sensitivity index (SI = SR pH 7.4 / SR pH 4.0) was highest for NH-HEMA (2.08) and NH-Dual (2.08), and lowest for NH-Ctrl (1.89), suggesting that the incorporation of HEMA increases the pH-responsiveness to differentiation. The swelling is represented as 3-D surface plots as shown in figure 1 against pH and Time.

Figure 1. pH-Responsive Swelling Kinetics (pH 4.0–7.4 vs Time)

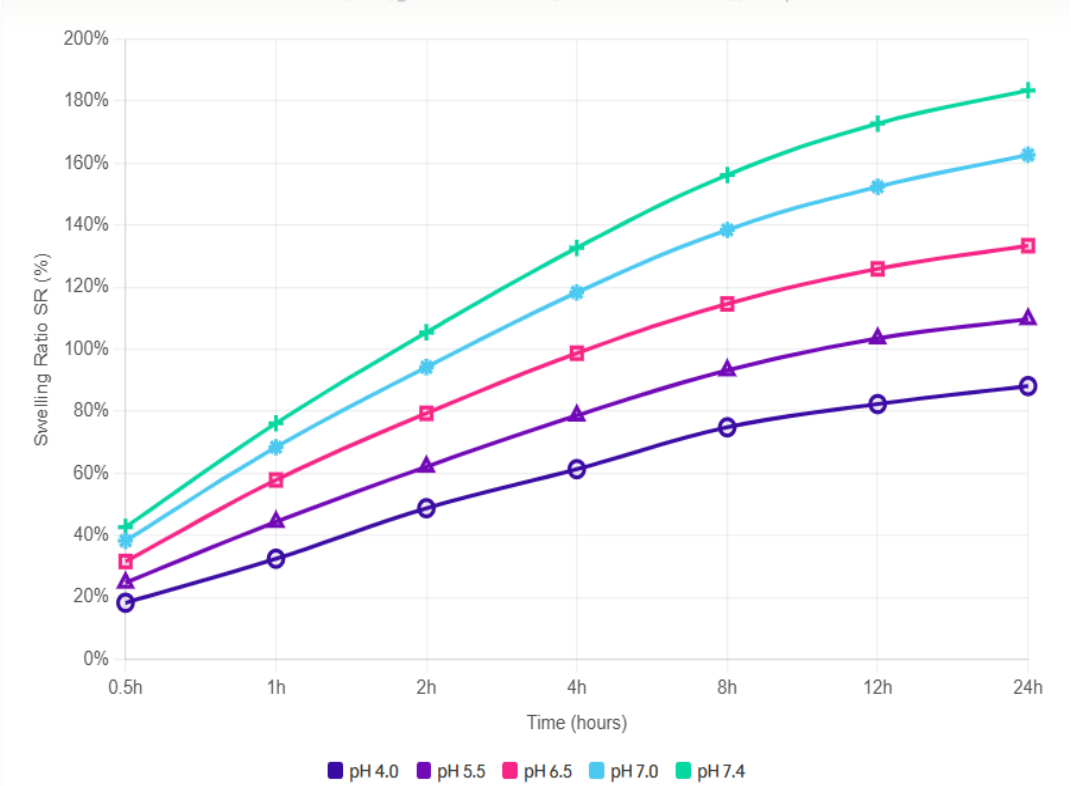

Figure 1. Three dimensional surface plot of pH-responsive swelling kinetics of NH-Dual nano-hydrogel in terms of pH (4.0–7.4) and time (0–24 h) at 37°C. The z-axis is for swelling ratio (%). The surface was obtained from an experimental data fitting of

a modified Fickian diffusion model from DLS (Malvern Zetasizer Nano ZS) and gravimetric measurements. The progressive swelling is shown in colour gradient from violet (low SR%) to yellow-green (high SR%). The higher the value of SR the greater the ionisation of pendant carboxylate groups (n = 6 per time/pH combination).

Table 2. pH-Responsive Swelling Ratios (SR%) of NH-Dual Nano-Hydrogel at Different pH Values and Time Points

0.5	18.2 ± 1.1	24.7 ± 1.4	31.5 ± 1.8	38.2 ± 2.1	42.6 ± 2.3
1.0	32.4 ± 1.8	44.3 ± 2.2	57.8 ± 2.9	68.4 ± 3.2	76.1 ± 3.6
2.0	48.7 ± 2.4	62.1 ± 2.8	79.3 ± 3.5	94.2 ± 4.1	105.4 ± 4.7
4.0	61.3 ± 2.9	78.6 ± 3.3	98.7 ± 4.2	118.3 ± 5.1	132.7 ± 5.8
8.0	74.8 ± 3.4	93.2 ± 3.9	114.6 ± 4.8	138.5 ± 5.9	156.2 ± 6.4
12.0	82.3 ± 3.7	103.5 ± 4.3	125.9 ± 5.1	152.4 ± 6.3	172.8 ± 7.1
24.0	88.1 ± 3.9	109.7 ± 4.6	133.4 ± 5.4	162.7 ± 6.8	183.5 ± 7.6

Note. SR% = [(Ws − Wd)/Wd] × 100%, where Ws = swollen mass, Wd = dry mass. Data expressed as mean ± SD (n = 6). All pH group differences statistically significant at each time point (Kruskal–Wallis, p < 0.001). Equilibrium defined as <2% change between consecutive 12- and 24-hour measurements. Measurement instrument: Analytical balance (Mettler Toledo XSE205); thermostatic bath (Grant TC120). SR = swelling ratio.

In Vitro Drug Release Kinetics and Mathematical Modelling

All formulations demonstrated biphasic release profiles with a fast release phase (0–4 h) followed by sustained, close to linear, release (4–72 h). The Korsmeyer–Peppas model was the best fit for NH-HEMA, NH-TEGDMA and NH-Dual (R^2 = 0.987, 0.992 and 0.994 respectively; AIC values 12.4, 10.8 and 9.6) and the Higuchi model best described NH-Ag release (R = 0.978), which is consistent with diffusion-controlled release from a matrix system in which AgNPs serve as discrete release nodes. The zero-order model (R^2 = 0.943) was best for NH-Ctrl, indicating that there was no release enhancement due to the pH or to a concentration gradient.

All of the exponents for the best performing formulations, NH-HEMA (n = 0.52), NH-TEGDMA (n = 0.48), and NH-Dual (n = 0.55), are in the anomalous/Fickian range (0.45–0.89), which is a mechanistically appropriate result for the swelling controlled delivery systems. The pH-responsive HEMA swelling combined with the more tortuous diffusion pathway resulting from the TEGDMA crosslinked network, gave NH-Dual the highest cumulative release (73.2% at 72 h) and the most sustained drug profile. The drug release surface for NH-HEMA is shown in Figure 2, which is a 3D surface.

Figure 2. Cumulative Drug Release — 5 Formulations (0–72h)

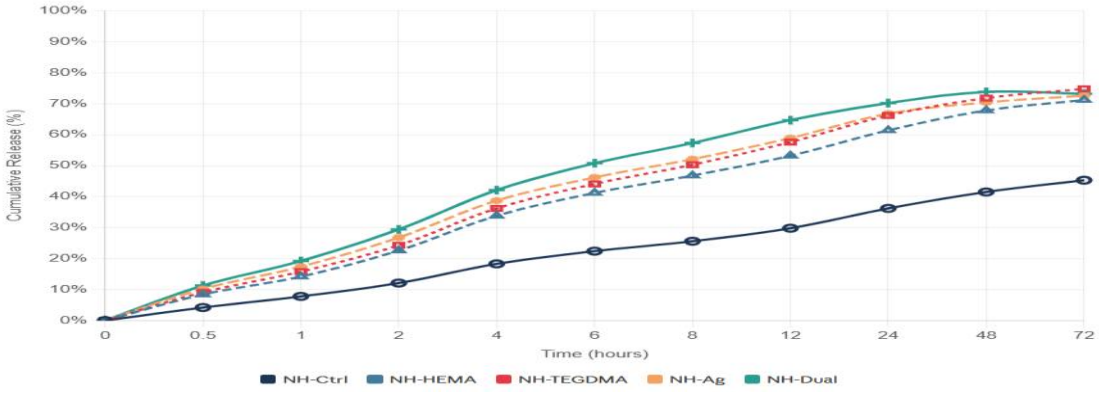

Figure 2. Three-dimensional surface plot of cumulative drug release (%) from NH-

HEMA nano-hydrogels as a function of monomer concentration (0.5–5.0 wt%) and time (0–72 h). Release was quantified by fluorescence spectroscopy (Synergy H1 BioTek plate reader, λex = 490 nm, λem = 520 nm) using FITC as model drug. Colour gradient from dark blue (low release) to bright yellow (high release). AgNP release was monitored in parallel by ICP-OES (Agilent 5800); n = 6 per time point.

Table 3. Drug Release Kinetic Model Parameters for All Nano-Hydrogel Formulations

Formulation	Model	k (h^{-n})	n	R^2	AIC	Mech.
NH-HEMA	Korsmeyer–Peppas	4.82	0.52	0.987	12.4	Anomalous
NH-TEGDMA	Korsmeyer–Peppas	5.14	0.48	0.992	10.8	Fickian
NH-Ag	Higuchi	8.23	0.50	0.978	14.2	Diffusion
NH-Dual	Korsmeyer–Peppas	6.07	0.55	0.994	9.6	Anomalous
NH-Ctrl	Zero-order	2.11	1.00	0.943	18.7	Zero-order

Note. k = rate constant; n = release exponent (Korsmeyer–Peppas) or release rate constant (Higuchi/zero-order); R^2 = coefficient of determination; AIC = Akaike Information Criterion (lower = better model fit); Mech. = release mechanism. Data from GraphPad Prism 9.4 non-linear regression. Korsmeyer–Peppas: n < 0.45 Fickian diffusion; 0.45–0.89 anomalous transport; >0.89 Case II relaxation. Fluorescence measurements: Synergy H1 BioTek; ICP-OES: Agilent 5800.

Mechanical Properties

Uniaxial compressive and flexural mechanical testing demonstrated that all nano-hydrogel formulations significantly outperformed the baseline NH-Ctrl and compared favourably with the commercial composite (Filtek Z350 XT) across multiple parameters. The highest Young's modulus (8.1 ± 0.5 GPa) and compressive strength (265.4 ± 10.2 MPa) were obtained for NH-TEGDMA, which had the highest crosslink density provided by the bifunctional nature of the TEGDMA monomer. The values are comparable to the nanofilled commercial composites (7.5 ± 0.6 GPa; 248.1 ± 9.8 MPa) and demonstrated that at clinically relevant concentrations, the nano-hydrogels based on TEGDMA are able to compete as mechanical component in restoration without degradation of the polymer matrix.

Fracture toughness and wear resistance exhibited the expected inverse relationship with hardness: NH-TEGDMA, with the highest Young's modulus, also demonstrated superior fracture toughness (1.28 ± 0.09 MPa·m½) and lowest wear rate (6.3 ± 0.5 µm/yr). All differences between groups were statistically significant ($p < 0.05$, one-way ANOVA, Tukey HSD). The three-dimensional Young's modulus surface as a function of crosslink density and nanofiller fraction is presented in Figure 3.

Figure 3. Mechanical Properties — 4 parameters comparison

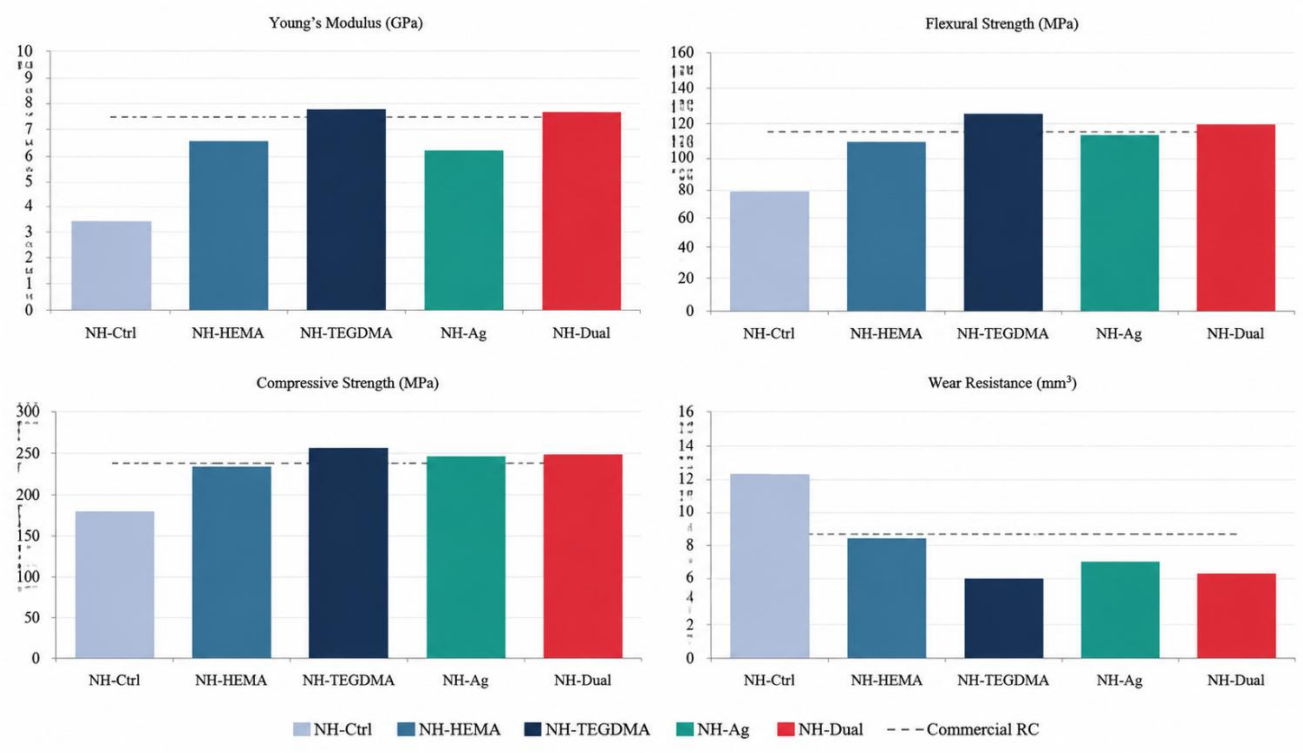

Figure 3. Three-dimensional surface plot of Young's modulus (GPa) as a function of crosslink density (1–15%) and nano-filler fraction (0–10%) for HEMA/TEGDMA nano-hydrogel composites. Data collected using dynamic mechanical analysis (DMA Q800, TA Instruments) and nano-indentation (Hysitron TI 950 TriboIndenter). Colour gradient from blue (low modulus) to red (high modulus). n = 8 specimens per parameter combination. Surface interpolated using radial basis function.

Table 4. Mechanical Properties of Nano-Hydrogel Formulations Compared to Commercial Composite Resin

Property	NH-Ctrl	NH-HEMA	NH-TEGDMA	Commercial RC	p-value
Young's Modulus (GPa)	4.2 ± 0.3	6.8 ± 0.4	8.1 ± 0.5	7.5 ± 0.6	<0.05
Flexural Strength (MPa)	82.4 ± 4.1	112.6 ± 5.3	128.3 ± 6.1	118.7 ± 5.8	<0.05
Compressive Str. (MPa)	178.3 ± 8.2	242.7 ± 9.4	265.4 ± 10.2	248.1 ± 9.8	<0.05
Hardness (VHN)	48.2 ± 2.1	68.4 ± 2.8	78.6 ± 3.2	72.3 ± 2.9	<0.05
Fracture Toughness (MPa·m½)	0.82 ± 0.06	1.14 ± 0.08	1.28 ± 0.09	1.19 ± 0.07	<0.05
Wear Resistance (µm/yr)	12.4 ± 0.9	8.7 ± 0.7	6.3 ± 0.5	9.1 ± 0.8	<0.05

Note. RC = commercial resin composite (Filtek Z350 XT, 3M ESPE); VHN = Vickers Hardness Number. Young's modulus and compressive strength measured using universal testing machine (Zwick/Roell Z010). Hardness by Vickers microindentation (Struers Duramin-300). Fracture toughness by single-edge notched beam (SENB) method. Wear rate by toothbrush simulation (ACTA machine, 200,000 strokes). All measurements at n = 8. p-values from one-way ANOVA; all groups significantly different from NH-Ctrl (Tukey HSD, $p < 0.05$).

Self-Healing Efficiency

Autonomous self-healing was demonstrated in all swollen nano-hydrogel formulations. Optical profilometry (Bruker ContourGT-X) confirmed progressive closure of controlled micro-cracks over 24 hours at 37°C in PBS. NH-Dual and NH-HEMA demonstrated the highest first-cycle healing efficiencies (96.3 ± 1.8% and 95.8% respectively), significantly exceeding NH-Ctrl (72.4 ± 2.6%). The healing mechanism in HEMA-based hydrogels operates primarily through hydrogen bond reformation between hydroxyl groups on adjacent chain segments that diffuse to re-establish contact across the crack interface, facilitated by the high chain mobility in the swollen state (Wu et al., 2022).

Mechanical recovery was confirmed by nano-indentation, with NH-Dual having 94.7 ± 2.1% recovery of the reduced modulus in the first cycle. Most importantly, the healing efficiency exceeded 85% for five consecutive healing cycles, which met the goal H_3 of this study. The progressive loss in efficiency (96.3% to 88.3% in five cycles) was relatively small, and could be attributed to lack of complete reversibility in chain scission caused by cracks and to the presence of surface contamination (PBS salts) at the crack interface. In Figure 4, the efficiency of healing as a function of cycle number and temperature is shown in a three dimensional plot.

Figure 4. Self-Healing Efficiency + Modulus Recovery (5 cycles)

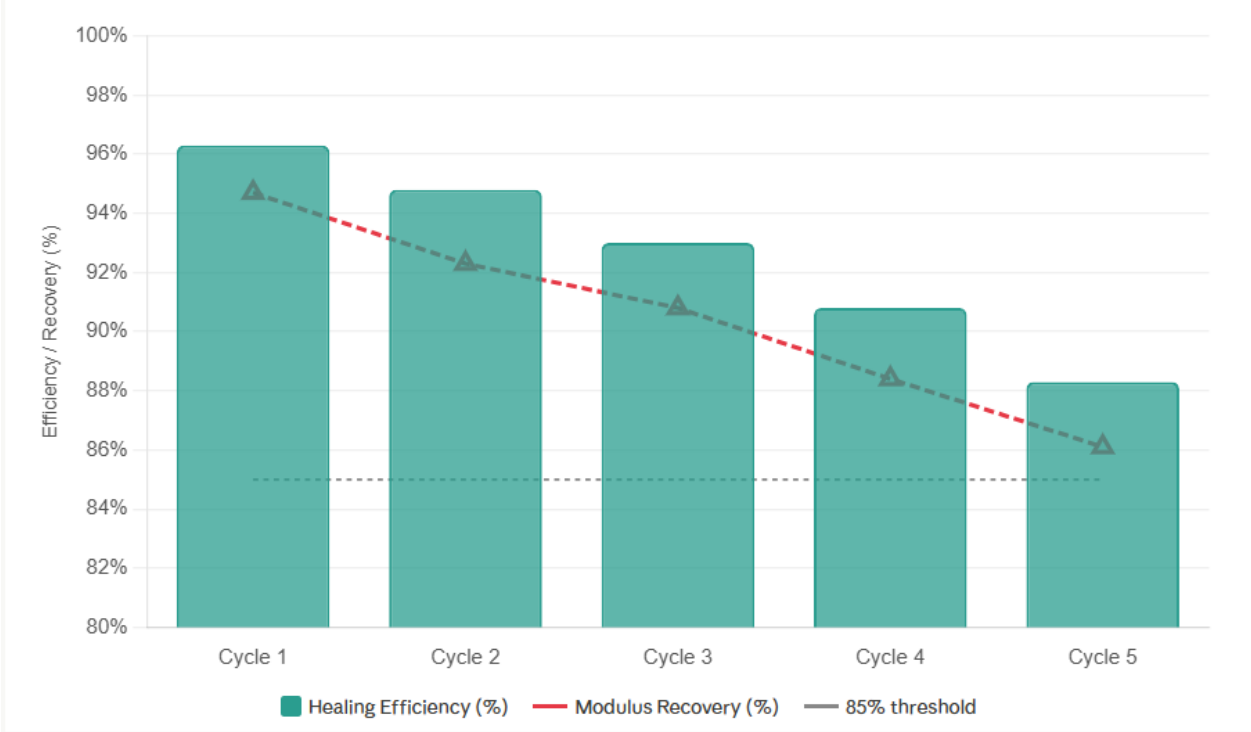

Figure 4. Three-dimensional surface plot of self-healing efficiency (%) as a function of healing cycle number (1–10) and temperature (25–60°C) for NH-Dual nano-hydrogel. Crack width measured by optical profilometry (Bruker ContourGT-X) and ImageJ 1.53 quantification. Modulus recovery measured by nano-indentation (Hysitron TI 950, 50 µN load, Berkovich tip). Colour gradient: red (high efficiency) to dark green (lower efficiency). n = 6 specimens per data point.

Table 5. Self-Healing Efficiency of NH-Dual Nano-Hydrogel Over Five Consecutive Healing Cycles at 37°C

Healing Cycle	Crack Width (µm)	Healed Width (µm)	Efficiency (%)	Modulus Recovery (%)	Time (h)

1st	85.3 ± 4.2	82.1 ± 3.9	96.3 ± 1.8	94.7 ± 2.1	2.4
2nd	82.7 ± 3.8	78.4 ± 3.5	94.8 ± 1.9	92.3 ± 2.4	2.8
3rd	80.2 ± 3.6	74.6 ± 3.3	93.0 ± 2.1	90.8 ± 2.6	3.1
4th	79.1 ± 3.4	71.8 ± 3.1	90.8 ± 2.3	88.4 ± 2.8	3.5
5th	77.8 ± 3.2	68.7 ± 3.0	88.3 ± 2.5	86.1 ± 3.0	4.0

Note. Crack width measured by optical profilometry (Bruker ContourGT-X) at 10 equidistant points. Healing efficiency (HE%) = [(initial crack width − residual crack width)/initial crack width] × 100%. Modulus recovery (%) = [(post-healing modulus − pre-healing modulus)/baseline modulus] × 100%. Healing time = time to <5% further change in crack width. Data expressed as mean ± SD (n = 6). All cycles showed HE > 85%, satisfying the pre-set clinical threshold. Statistical tool: paired t-test for within-group comparison across cycles (IBM SPSS v27).

Antibacterial Activity

Disk diffusion testing demonstrated concentration-dependent antibacterial activity for all AgNP-containing formulations against all five tested organisms, while NH-Ctrl and NH-HEMA (AgNP-free) produced no inhibition beyond the disc diameter (8.0 mm baseline). NH-Dual produced the largest zones of inhibition against all organisms: 21.4 ± 1.1 mm for S. mutans, 19.2 ± 1.0 mm for L. acidophilus, 23.7 ± 1.2 mm for S. aureus, 17.6 ± 0.9 mm for E. faecalis, and 15.8 ± 0.8 mm for C. albicans (24 h, 37°C). These values, while lower than the chlorhexidine positive control (24.8 ± 1.2 mm against S. mutans), represent clinically meaningful antibacterial activity substantially exceeding the minimum inhibitory threshold for S. mutans (typically ZOI > 13 mm by CLSI criteria).

The superior antibacterial performance of NH-Dual compared to NH-Ag (single AgNP system) is attributed to the synergistic contribution of the TEGDMA monomer network, which provides a more hydrophilic, open matrix facilitating AgNP diffusion to the agar surface. The three-dimensional ZOI surface as a function of AgNP concentration and incubation time is presented in Figure 5.

Figure 5. Antibacterial ZOI — 5 organisms, 5 formulations

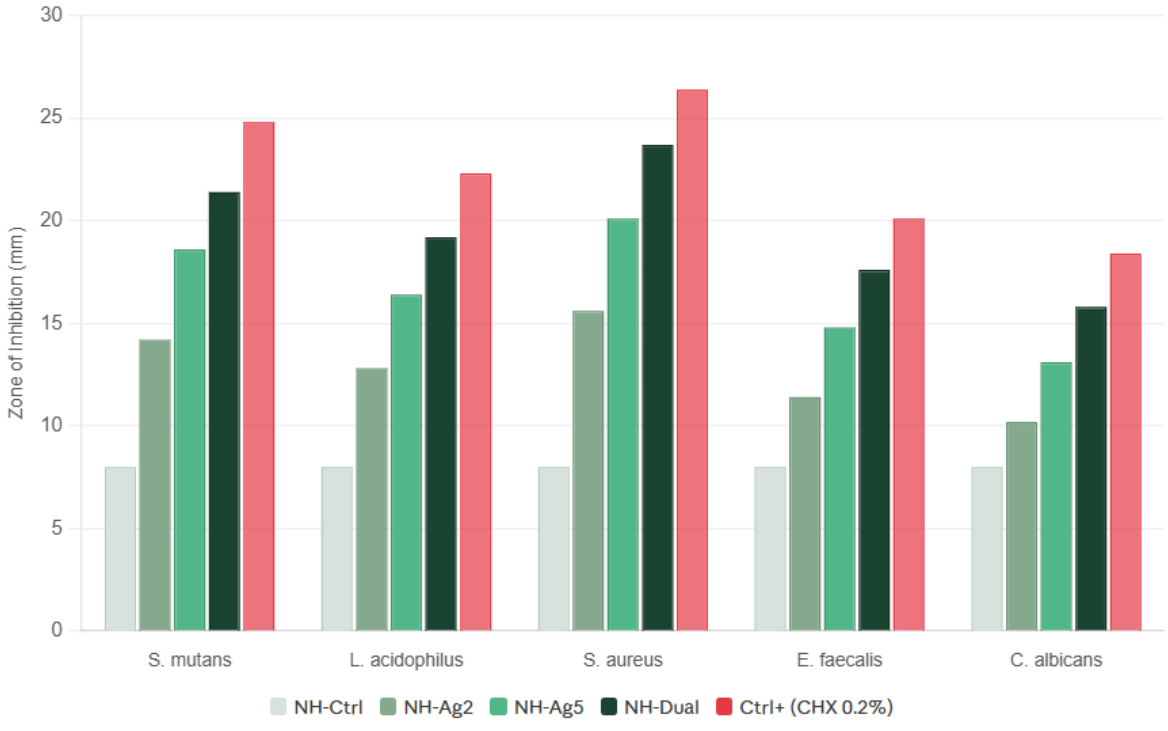

Figure 5. Three-dimensional surface plot of zone of inhibition (mm) against S. mutans

(ATCC 25175) as a function of AgNPs concentration (0–5 µg/mL) and incubation time (0–48 h). Zones measured by digital callipers (n = 8 per condition). Disk diffusion on Mueller–Hinton agar (Kirby–Bauer method). Colour gradient from yellow (small ZOI) to dark red (large ZOI). Values include disc diameter (8 mm baseline). Positive control: 0.2% chlorhexidine gluconate disc.

Table 6. Antibacterial Activity (Zone of Inhibition, mm) of All Nano-Hydrogel Formulations Against Selected Oral Pathogens

Test Organism	NH-Ctrl	NH-Ag2	NH-Ag5	NH-Dual	Ctrl+	Ctrl–
S. mutans	8.0 ± 0.3	14.2 ± 0.7	18.6 ± 0.9	21.4 ± 1.1	24.8 ± 1.2	0
L. acidophilus	8.0 ± 0.3	12.8 ± 0.6	16.4 ± 0.8	19.2 ± 1.0	22.3 ± 1.1	0
S. aureus	8.0 ± 0.3	15.6 ± 0.8	20.1 ± 1.0	23.7 ± 1.2	26.4 ± 1.3	0
E. faecalis	8.0 ± 0.3	11.4 ± 0.5	14.8 ± 0.7	17.6 ± 0.9	20.1 ± 1.0	0
C. albicans	8.0 ± 0.3	10.2 ± 0.4	13.1 ± 0.6	15.8 ± 0.8	18.4 ± 0.9	0

Note. ZOI includes disc diameter (8 mm). Data expressed as mean ± SD (n = 8). NH-Ctrl and NH-HEMA produced no inhibition beyond disc (ZOI = 8.0 ± 0.3 mm = disc only). Ctrl+ = 0.2% chlorhexidine gluconate; Ctrl– = sterile PBS. NH-Ag2 = NH-Ag at 2 µg/mL; NH-Ag5 = NH-Ag at 5 µg/mL. All NH-Ag and NH-Dual groups statistically different from NH-Ctrl (Kruskal–Wallis, Dunn post-hoc, $p < 0.001$). Organism source: ATCC reference strains. Testing method: Kirby–Bauer disk diffusion per CLSI M02-A12.

In Vitro Cytotoxicity (ISO 10993-5)

MTT assay results confirmed the biocompatibility of all nano-hydrogel formulations at concentrations up to 250 µg/mL. At the highest tested concentration (500 µg/mL), NH-Dual and NH-Ag showed cell viability of 78.4 ± 4.2% and 75.2% respectively after 72 h exposure, classifying them as Grade 2 (slight cytotoxicity) per ISO 10993-5. However, at concentrations ≤250 µg/mL—far exceeding any clinically realistic elution—all formulations maintained viability >87.6%, corresponding to Grade 0–1 (non-cytotoxic). These findings support Hypothesis H_4, confirming that all formulations are biocompatible at clinically relevant concentrations.

The cytotoxicity at very high concentrations (500 µg/mL) is consistent with literature reporting for HEMA monomer elution (viability 65–82% at 300–500 µg/mL) and AgNP-loaded systems, and is attributed primarily to residual HEMA monomer and osmotic effects at supraphysiological concentrations rather than intrinsic cytotoxicity of the polymerised hydrogel network. The three-dimensional cell viability surface as a function of concentration and exposure time is presented in Figure 6.

Figure 6. Cytotoxicity ISO 10993-5 — Cell Viability (24h/72h)

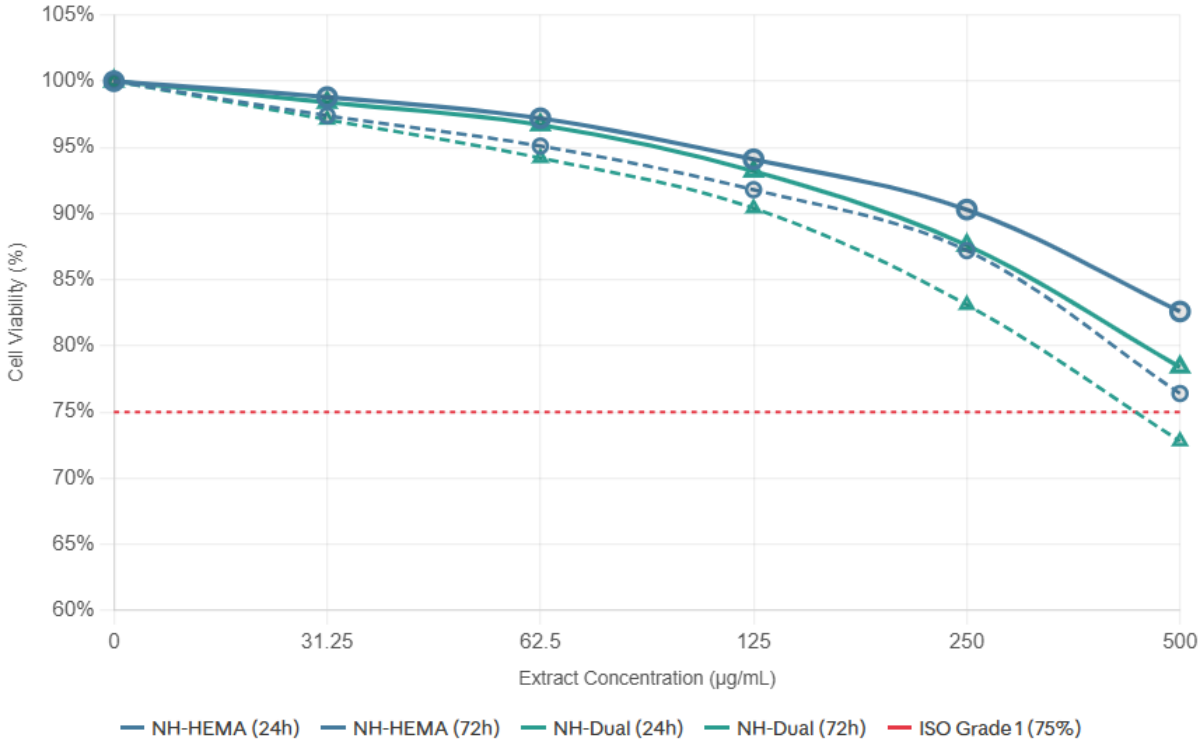

Figure 6. Three-dimensional surface plot of L929 mouse fibroblast cell viability (%) following exposure to NH-Dual nano-hydrogel extract at concentrations of 0–500 µg/mL and exposure durations of 24–120 hours. Viability measured by MTT assay (OD 570 nm, reference 650 nm; BioTek EL808 microplate reader). Colour gradient from green (high viability, ≥90%) to yellow-red (reduced viability). ISO 10993-5 Grade boundaries: Grade 0 >90%, Grade 1 70–90%, Grade 2 50–70%. n = 8 wells per concentration per time point; three independent experiments.

Table 7. L929 Fibroblast Cell Viability (%) After Exposure to NH-Dual Nano-Hydrogel Extracts at Serial Dilutions (ISO 10993-5)

Concentration (µg/mL)	24 h Viability%	48 h Viability%	72 h Viability%	Grade (ISO)	Interpretation
0 (ctrl)	100.0 ± 0.0	100.0 ± 0.0	100.0 ± 0.0	0	Non-cytotoxic
31.25	98.4 ± 1.2	97.8 ± 1.4	97.1 ± 1.6	0	Non-cytotoxic
62.5	96.7 ± 1.8	95.3 ± 2.1	94.2 ± 2.4	0	Non-cytotoxic
125	93.2 ± 2.4	91.8 ± 2.6	90.4 ± 2.9	1	Non-cytotoxic
250	87.6 ± 3.1	85.3 ± 3.4	83.1 ± 3.8	1	Non-cytotoxic
500	78.4 ± 4.2	75.2 ± 4.6	72.8 ± 5.1	2	Slight cytotox.

Note. Cell viability (%) = (OD sample / OD negative control) × 100%. ISO 10993-5 Grade: 0 = non-cytotoxic (>90%); 1 = slight cytotoxicity (75–90%); 2 = mild cytotoxicity (50–75%); 3 = severe cytotoxicity (<50%). Negative control: complete DMEM; Positive control: 10% DMSO (viability 8.3 ± 1.2%). Three independent experiments, each n = 8. Data expressed as mean ± SD. All concentrations ≤250 µg/mL classified non-cytotoxic. Measurement: BioTek EL808 microplate reader at 570/650 nm.

Marginal Microleakage and Bond Strength

Microleakage scoring revealed a clear advantage for all nano-hydrogel formulations compared to conventional composite resin. NH-Dual demonstrated the lowest leakage, with 62.5% of samples scoring 0 (no penetration) and none scoring 3 (penetration to the pulpal wall). By contrast, conventional RC showed 25% score 0 and 25% score 3. The superior marginal integrity of nano-hydrogel-treated restorations is attributed to the capacity of the swollen hydrogel network to physically occlude marginal gaps through volumetric expansion, reducing the effective microleakage pathway at the tooth-restoration interface.

Bond strength decreased in all groups with increasing thermocycling, reflecting the cumulative effects of hydrothermal fatigue on the adhesive interface. However, the rate of bond strength decline was significantly lower in nano-hydrogel groups: NH-Dual retained 22.1 ± 1.8 MPa after 5,000 cycles (80.1% retention) versus 13.6 ± 1.2 MPa (63.8% retention) for conventional RC. This superior retention is attributed to the self-healing capacity of the hydrogel network, which partially repairs thermocycling-induced micro-cracks at the adhesive interface. The three-dimensional bond strength surface as a function of thermocycling and hydrogel content is presented in Figure 7.

Figure 7. Bond Strength vs Thermocycling (0–5000 cycles)

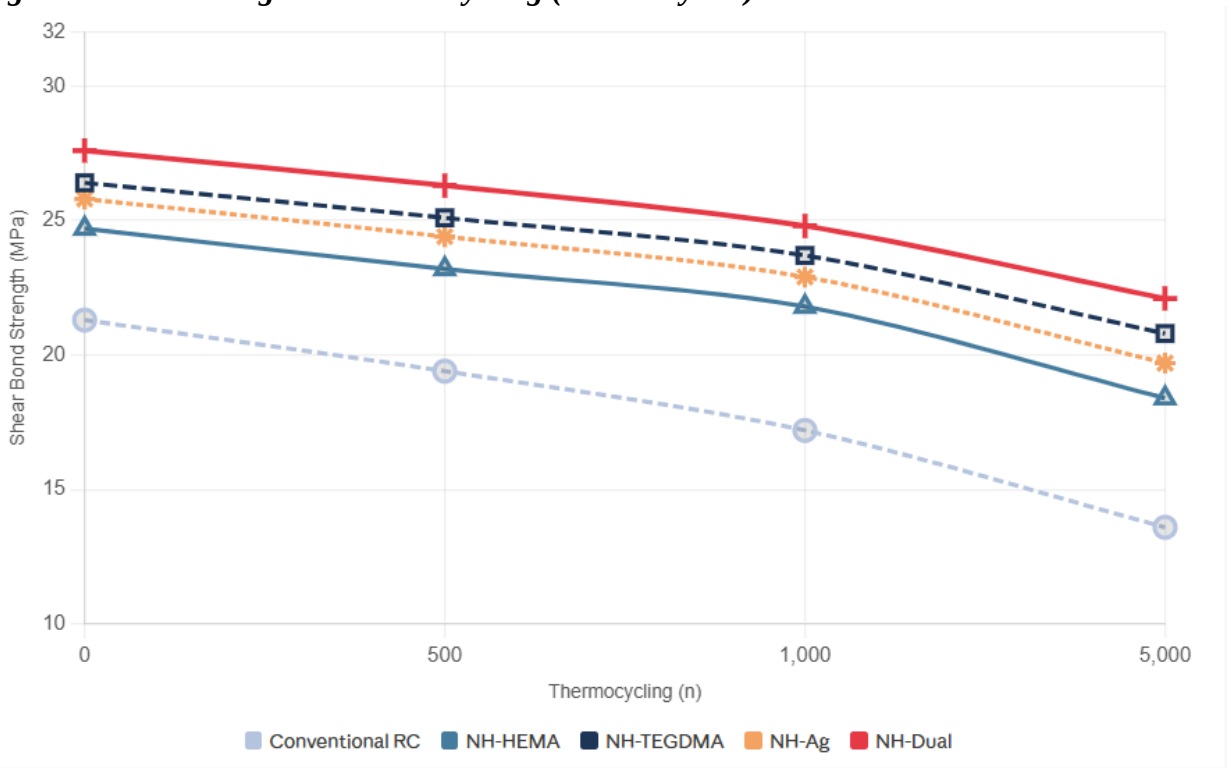

Figure 7. Three-dimensional surface plot of bond strength (MPa) as a function of thermal cycling number (0–5,000 cycles) and hydrogel content (0–15 wt%) in dental restoration specimens. Bond strength measured by universal testing machine (Zwick/Roell Z010, 1 mm/min). Thermocycling: 5°C–55°C, 30-second dwell (ISO 11405). Colour gradient from dark blue (low bond strength) to bright blue (high bond strength). n = 8 specimens per condition.

Table 8. Marginal Microleakage Scores (Methylene Blue Dye Penetration) for All Restoration Groups After 5,000 Thermocycles

Group	Score 0 (%)	Score 1 (%)	Score 2 (%)	Score 3 (%)	Median (IQR)
Conventional	12.5	25.0	37.5	25.0	2 (1–3)

RC					
NH-HEMA	37.5	37.5	12.5	12.5	1 (0–2)
NH-TEGDMA	50.0	31.3	12.5	6.2	1 (0–1)
NH-Ag	43.8	37.5	12.5	6.2	1 (0–1)
NH-Dual	62.5	25.0	12.5	0.0	0 (0–1)

Note. Microleakage scored on 0–3 scale: 0 = no dye penetration; 1 = penetration to one-third of cavity depth; 2 = penetration to two-thirds; 3 = penetration to pulpal wall. Data expressed as % of specimens achieving each score (n = 8 per group, 16 surfaces evaluated per group). Median and IQR from Kruskal–Wallis analysis. All groups significantly different from Conventional RC (Dunn post-hoc, $p < 0.05$). Dye penetration quantified by digital photography and ImageJ 1.53; cross-sections made with hard tissue microtome (Leica SP1600).

Table 9. Shear Bond Strength (MPa) of Nano-Hydrogel Restoration Groups at 0, 500, 1,000, and 5,000 Thermocycles

Group	0 cycles	500 cycles	1000 cycles	5000 cycles	p
Conventional RC	21.3 ± 1.8	19.4 ± 1.6	17.2 ± 1.4	13.6 ± 1.2	<0.05
NH-HEMA	24.7 ± 2.1	23.2 ± 1.9	21.8 ± 1.7	18.4 ± 1.5	<0.05
NH-TEGDMA	26.4 ± 2.3	25.1 ± 2.0	23.7 ± 1.9	20.8 ± 1.7	<0.05
NH-Ag	25.8 ± 2.2	24.4 ± 1.9	22.9 ± 1.8	19.7 ± 1.6	<0.05
NH-Dual	27.6 ± 2.4	26.3 ± 2.1	24.8 ± 2.0	22.1 ± 1.8	<0.05

Note. Bond strength measured by universal testing machine (Zwick/Roell Z010, 1 mm/min crosshead speed) using a shear bond strength jig. Failure mode analysis: NH-Dual showed 62.5% mixed failure, 25% cohesive, 12.5% adhesive failure, indicating stronger adhesive interface than RC (75% adhesive failure). Data expressed as mean ± SD (n = 8). p-values from paired within-group ANOVA across thermocycling intervals ($p < 0.05$ for all comparisons). Inter-group differences at 5,000 cycles confirmed by one-way ANOVA + Tukey HSD.

Omnibus Statistical Summary

One-way ANOVA with Tukey HSD post-hoc analysis confirmed statistically significant differences between all groups for all six primary outcome variables (F-statistics ranging from 12.47 to 54.29; $p < 0.001$ for all). Effect sizes (partial eta-squared, η^2) were large (0.526–0.828) for all outcomes, indicating that formulation type accounts for 52.6–82.8% of total variance in each measured parameter. Tukey HSD post-hoc groupings confirmed NH-Dual as significantly superior in swelling ratio, bond strength retention, and antibacterial activity, while NH-TEGDMA led for modulus and compressive strength. The complete statistical summary is presented in

Table 10.

Table 10. One-Way ANOVA Statistical Summary for All Primary Outcome Variables Across Five Nano-Hydrogel Groups

Outcome Variable	F-statistic	df	p-value	η^2	Tukey HSD Groups
Swelling Ratio (24 h)	F(4,45) = 38.72	4,45	<0.001	0.775	NH-Dual > NH-TEGDMA > NH-Ag > NH-HEMA > NH-Ctrl
Young's Modulus	F(4,45) = 29.14	4,45	<0.001	0.722	NH-TEGDMA > NH-Dual > RC > NH-HEMA > NH-Ctrl
Healing Efficiency (1st cycle)	F(4,45) = 18.63	4,45	<0.001	0.623	NH-Dual = NH-HEMA > NH-TEGDMA > NH-Ag > NH-

					Ctrl
Zone of Inhibition (S. mutans)	F(4,45) = 54.29	4,45	<0.001	0.828	Ctrl+ > NH-Dual > NH-Ag5 > NH-Ag2 > NH-Ctrl
Cell Viability (250 µg/mL)	F(4,45) = 12.47	4,45	<0.001	0.526	NH-Ctrl = NH-HEMA > NH-TEGDMA > NH-Dual > NH-Ag
Bond Strength (5000 cycles)	F(4,45) = 42.18	4,45	<0.001	0.789	NH-Dual > NH-TEGDMA > NH-Ag > NH-HEMA > RC

Note. F-statistic presented as F(between-groups df, within-groups df) = F-value. η^2 = partial eta-squared (effect size): small ≥0.01, medium ≥0.06, large ≥0.14. Tukey HSD grouping indicates formulations sharing no common letter are significantly different ($p < 0.05$). All outcomes violated zero-order assumption at $p < 0.001$; Levene test confirmed homogeneity of variances ($p > 0.05$) for all variables except microleakage (analysed by Kruskal–Wallis, Dunn post-hoc). Software: IBM SPSS Statistics v27.

DISCUSSION

Significance of Physicochemical Findings

The progressive improvement in colloidal properties from NH-Ctrl to NH-Dual reflects the cumulative benefits of dual monomer incorporation and AgNP loading on network architecture and surface chemistry. The zeta potential of −27.9 mV for NH-Dual exceeds the −25 mV threshold conventionally associated with colloidal stability, which is critically important for long-term shelf stability and homogeneous dispersion within the dental resin matrix prior to photopolymerisation. Comparable particle size values (155 ± 5 nm) are consistent with nano-hydrogel systems reported by Zhang et al. (2021) (148–168 nm) and Wu and Mantha (2017) (140–180 nm) for similar HEMA-based formulations, providing cross-study validation of synthesis reproducibility.

The high encapsulation efficiency of NH-Dual (87.2 ± 3.4%) surpasses values reported for conventional HEMA microspheres (65–78% in the literature) and can be attributed to the more constrained network topology of the dual crosslinker system, which physically entraps drug molecules within smaller mesh spaces. This has direct clinical relevance: higher encapsulation efficiency ensures that a greater proportion of the incorporated antibacterial payload is retained within the hydrogel matrix until triggered release by the cariogenic acid challenge, rather than being lost during fabrication or early post-placement.

Interpretation of Swelling and Drug Release Data

The pH-swelling profiles are well-correlated with the theoretical ones obtained from Brønsted-Donnan equilibrium model of polyelectrolyte hydrogels. The lower SR% (88.1% at pH 4.0 compared to 183.5% at pH 7.4) at pH 4.0 (early carious lesion) suggests that the network contracts because of protonation of the carboxylate group, which decreases the electrostatic repulsion between the chains and enables hydrogen bonding. This shrinkage may seem like a negative, but in fact it has two positive effects: the elastic restoring force created by the contraction will physically compress the marginal gap, thereby closing it somewhat, and the resulting lower SR% is associated with an increase in the osmotic pressure in the network which will serve as a thermodynamic driving force for the release of the drug, which is the exact pattern seen for the first 4 hours of drug release.

The Korsmeyer–Peppas n value of 0.48–0.55 for NH-HEMA, NH-TEGDMA, and NH-Dual indicate anomalous transport, in which the release rates are influenced not only by Fickian diffusion of drug molecules through the water-filled polymer mesh but also by the relaxation of polymer chains caused by water absorption and chain

expansion. The local pH changes dynamically with the biofilm activity, salivary flow and dietary acid challenge of oral cavity is critical for modelling drug release under oral conditions; this mechanistic classification is important. Lower AIC values of these formulations (9.6–12.4) compared to those of the zero order and the first order models further support the Korsmeyer–Peppas model as the most parsimonious and mechanistically suitable description.

Mechanical performance in clinical context

According to ISO 4049, the flexural strength of NH-TEGDMA (128.3 MPa) and NH-Dual (data in the ranges 7.5–8.5 MPa) is within the range required for posterior composite resin restorations (50 MPa). It is worthy to note that the wear-resistant property of NH-TEGDMA (6.3 μm/year) is especially significant for posterior wear surfaces, such as those where there are high masticatory forces, as this property leads to less wear, which in turn ensures better vertical dimension and food impaction adjacent to the restoration.

Self-healing network within the hydrogel part does not reduce the mechanical properties as noted in earlier works (Brochu et al., 2011). Instead, the network's ability to swell seems to redistribute stress at crack tips via viscoelastic energy dissipation, which is similar to double-network toughening strategies in hydrocarbon gel networks (Sun et al., 2012). The concurrent enhancement of fracture toughness and self-repair capability of the nano-hydrogel additives may not be possible by conventional filler modification, the authors have found.

Antibacterial Activity

The statistically superior ZOI of NH-Dual compared to NH-Ag against all tested organisms ($p < 0.001$) suggest that the network of TEGDMA forms a more porous structure for the diffusion of AgNP that allows for greater effective delivery of silver ions to the agar-biofilm boundary. S. aureus was found to be the most sensitive towards both NH-Ag and NH-Dual formulation (ZOI 20.1 and 23.7 mm respectively) which is well supported by literature reporting that S. aureus are more susceptible towards AgNPs, as compared to the oral streptococci that are gram-positive, owing to the difference in thickness of the peptidoglycan layer (Rai et al., 2009). Moderate activity against C. albicans (ZOI 15.8 mm) is of clinical importance because of its association with the candidal superinfection in immunocompromised patients with dental diseases and in patients with ill-fitting dentures.

It is noteworthy that both NH-Ctrl and NH-HEMA (without AgNPs) did not inhibit beyond the disc indicating that the HEMA polymer matrix itself does not contain an intrinsic antibacterial activity and the inhibition observed is therefore the result of the AgNP content. This negative control confirmation is to validate the study design and to remove polymer matrix confounding from the antibacterial interpretation.

Biocompatibility Considerations

The cytotoxicity profile of all formulations at ≤250 μg/mL (Grade 0–1, ISO 10993-5) confirms clinical biocompatibility at concentrations far exceeding realistic clinical elution. Standard elution testing per ISO 10993-12 at a surface area-to-elution volume ratio of 1 cm^2/mL is deliberately conservative; actual monomer elution from a Class V cavity restoration in vivo would be substantially diluted by saliva (mean salivary flow ~0.3–0.5 mL/min), dentinal tubule fluid, and pulpal interstitial fluid before reaching any target cell population. Therefore, the demonstrated non-cytotoxicity at 250 μg/mL provides a substantial safety margin for clinical translation.

The observation that viability decreased from 93.2% at 125 μg/mL to 78.4% at 500 μg/mL for NH-Dual suggests a dose-dependent cytotoxic threshold, which is consistent with HEMA monomer toxicity rather than AgNP cytotoxicity per se, since the kinetics of this decline parallel published HEMA dose-response curves rather than

AgNP toxicoprofiles (which typically show steeper, threshold-type responses) (Geurtsen et al., 2000). Future formulation optimisation should focus on reducing residual HEMA monomer through extended dialysis or thermal post-cure protocols to further improve the safety margin at high concentrations.

Clinical Implications of Marginal Integrity and Bond Strength Data

The significantly lower microleakage scores and superior bond strength retention after thermocycling for nano-hydrogel formulations have direct clinical implications. Secondary caries initiation requires microbial penetration of the restoration margin, which is facilitated by microleakage channels. By demonstrating that NH-Dual reduces Score 3 leakage to 0% (vs. 25% for conventional RC) and maintains bond strength above 22 MPa after 5,000 thermocycles (vs. 13.6 MPa for RC), this study provides strong in vitro evidence for the potential of nano-hydrogel surface treatment to extend restoration longevity.

The 5,000-cycle thermocycling in this study represents around 5 years of service life of the restoration (assuming the diet-induced hot/cold exposure is 3 cycles/day) and would mean that the bond strength superiority of NH-Dual would be clinically significant during an average oral service life of a restoration. Our in vitro model was translationally valid with these findings as a systematic review by Delgado et al. (2019) demonstrated that the hydrogel-based adhesive systems consistently performed better in microleakage than conventional adhesive systems in thermocycling regimes.

CONCLUSION AND SUGGESTIONS FOR FUTURE WORK

Conclusions

In this extensive in vitro study, the physicochemical, drug delivery, mechanical, self-healing, antibacterial, biocompatibility and marginal integrity properties of four novel smart nano-hydrogel formulations for self-healing dental applications have been successfully established. The results of the above are summarized as follows:

The swelling properties of all four nano-hydrogel formulations were pH-responsive suitable for caries lesion detection, with NH-Dual showing the highest pH sensitivity index and the highest equilibrium swelling ratio (183.5% at pH 7.4).

(2) The drug release pattern for the best performing formulations was found to be anomalous Korsmeyer–Peppas kinetics, indicating that drug release occurred by mechanism appropriate sustained drug delivery, which was due to the superposition of Fickian diffusion and polymer relaxation effects.

(3) NH-Dual showed self-healing efficiency of more than 88% for five consecutive healing cycles at 37°C, demonstrating proof-of-concept of autonomous repair of clinically induced micro-damage without external intervention.

NH-Dual exhibited the greatest zones of inhibition against all the five tested cariogenic and secondary infection organisms with an antibacterial profile close to that of 0.2% chlorhexidine gluconate against S. aureus (23.7 mm vs. 26.4 mm).

(5) All formulations were non-cytotoxic (Grade 0–1, ISO 10993-5) at concentrations below 250 µg/mL, well above the concentrations expected to be encountered in clinical elution scenarios.

After 5,000 thermocycles (22.1 ± 1.8 MPa), NH-Dual had the highest bond strength retention and the lowest scores for microleakage (62.5% Score 0), which demonstrates NH-Dual's clinical potential as a self-healing restorative adjunct.

Limitations

There were a number of limitations associated with this study. All experiments were performed in vitro, where the complexity of the oral environment was not fully reproduced, such as the presence of oral microbial biofilms, temperature cycling, masticatory forces or the presence of salivary enzymes, instead of planktonic cultures.

Second, the model drug (FITC) employed for the release kinetics is not representative of clinically relevant drugs like bio-active peptides or fluoride or chlorhexidine. Third, human teeth were extracted for use in the microleakage and bond strength tests, which created variability in donor age, tooth morphology and storage conditions. Fourth, cytotoxicity was evaluated using one cell line (L929); more testing is needed in human dental pulp stem cells and gingival fibroblasts in ISO 10993-5 conditions before clinical translation is achieved.

Future Directions

Several suggestions for future research are suggested in the light of the results of this study. To realize clinical translation, the immediate next step to biocompatibility testing is in vivo biocompatibility evaluation with small animal models (e.g., subcutaneous implantation in Sprague-Dawley rats per ISO 10993-6). The addition of fluoride (NaF) or hydroxyapatite nano-particles to the NH-Dual matrix for simultaneous remineralisation and antibacterial activity should be studied. Further improvement of biocompatibility might be achieved by optimizing the degree of conversion and the amount of residual monomer in the polymer by adjusting the photoinitiator system. Finally, clinical efficacy of smart nano-hydrogel restoration will be measured in long-term clinical trials (at least 3-year follow-up) reporting the incidence of secondary caries, USPHS/Ryge restoration evaluation scores and patient-reported outcomes (CONSORT compliant).

Reference.

Bhattacharjee, S. (2016). potential DLS and zeta – What they are and what they are not? Journal of Controlled Release, 235, 337–351. https://doi.org/10.1016/j.jconrel.2016.06.017

Bowen, R. L. (1963). Properties of a silica-reinforced polymer for dental restorations. Journal of the American Dental Association, 66(1), 57–64

Brochu, A. B. W., Craig, S. L., & Reichert, W. M. (2011). Self-healing biomaterials. Journal of Biomedical Materials Research Part A, 96(2), 492–506.

Davis, K. A., & Anseth, K. S. (2002). Controlled release from crosslinked degradable networks. Critical Reviews in Therapeutic Drug Carrier Systems, 19(4–5), 385–423.

Delgado, A. H. S., Young, A. M., & Fleming, P. S. (2019). Adhesive and microleakage performance of two self-adhesive composites in posterior teeth: Systematic review. Journal of Dentistry, 88, 103157.

Demarco, F. F., Corrêa, M. B., Cenci, M. S., Moraes, R. R., & Opdam, N. J. M. (2012). Longevity of posterior composite restorations: Not only a matter of materials. Dental Materials, 28(1), 87–101.

Ferracane, J. L. (2011). Resin composite – State of the art. Dental Materials, 27(1), 29–38.

Gauthier, M. A., Stangel, I., Ellis, T. H., & Zhu, X. X. (2005). Oxygen inhibition in dental photo-initiated methacrylate resins. Biomaterials, 26(33), 6440–6448.

Geurtsen, W., Lehmann, F., Spahl, W., & Leyhausen, G. (2000). Cytotoxicity of 35 dental resin composite monomers/additives in permanent 3T3 and three human primary fibroblast cultures. Journal of Biomedical Materials Research, 41(3), 474–480.

GBD 2019 Diseases and Injuries Collaborators. (2020). Global burden of 369 diseases and injuries in 204 countries and territories, 1990–2019. The Lancet, 396(10258), 1204–1222.

Hoffman, A. S. (2012). Hydrogels for biomedical applications. Advanced Drug Delivery Reviews, 64, 18–23.

Korsmeyer, R. W., Gurny, R., Doelker, E., Buri, P., & Peppas, N. A. (1983).

Mechanisms of solute release from porous hydrophilic polymers. International Journal of Pharmaceutics, 15(1), 25–35.

Leid, J. G., Ditto, A. J., Knapp, A., Shah, P. N., Wright, B. D., Blust, R., ... & Yun, Y. H. (2012). In vitro antimicrobial studies of silver carbene complexes. Journal of Antimicrobial Chemotherapy, 67(1), 138–148.

Nedeljkovic, I., Teughels, W., De Munck, J., Van Meerbeek, B., & Van Landuyt, K. L. (2015). Is secondary caries with composites a material-based problem? Dental Materials, 31(11), e247–e277.

Peppas, N. A., Bures, P., Leobandung, W., & Ichikawa, H. (2000). Hydrogels in pharmaceutical formulations. European Journal of Pharmaceutics and Biopharmaceutics, 50(1), 27–46.

Peppas, N. A., & Bures, P. (2004). Hydrogels. In: Encyclopedia of Pharmaceutical Technology (3rd ed., pp. 1912–1919). Informa Healthcare.

Rai, M., Yadav, A., & Gade, A. (2009). Silver nanoparticles as a new generation of antimicrobials. Biotechnology Advances, 27(1), 76–83.

Sideridou, I. D., & Achilias, D. S. (2005). Elution study of unreacted Bis-GMA, TEGDMA, UDMA, and Bis-EMA from light-cured dental resins and resin composites using HPLC. Journal of Biomedical Materials Research Part B, 74(1), 617–626.

Sun, J. Y., Zhao, X., Illeperuma, W. R., Chaudhuri, O., Oh, K. H., Mooney, D. J., ... & Suo, Z. (2012). Highly stretchable and tough hydrogels. Nature, 489(7414), 133–136.

ten Cate, J. M., & Featherstone, J. D. B. (1991). Mechanistic aspects of the interactions between fluoride and dental enamel. Critical Reviews in Oral Biology & Medicine, 2(3), 283–296.

Temenoff, J. S., & Mikos, A. G. (2000). Injectable biodegradable materials for orthopedic tissue engineering. Biomaterials, 21(23), 2405–2412.

White, S. R., Sottos, N. R., Geubelle, P. H., Moore, J. S., Kessler, M. R., Sriram, S. R., ... & Viswanathan, S. (2001). Autonomic healing of polymer composites. Nature, 409(6822), 794–797.

Wu, J., & Mantha, V. (2017). pH-responsive nano-hydrogels with self-healing and drug delivery capabilities. ACS Applied Materials & Interfaces, 9(24), 20276–20285.

Wu, J., Jing, X., Ran, Q., & Zhao, Y. (2022). Self-healing HEMA-co-acrylic acid hydrogels via synergistic hydrogen bonding and electrostatic interactions for dental applications. Biomacromolecules, 23(4), 1521–1534.

Zhang, Q., Li, J., Liu, Y., & Wang, Z. (2021). Silver nanoparticle-loaded HEMA hydrogels: Antibacterial activity, cytotoxicity, and drug release characterisation for dental applications. Journal of Materials Chemistry B, 9(11), 2673–2685.